CLM-R 76

CLM-R 76

United Kingdom Atomic Energy Authority

RESEARCH GROUP

Report

COMPUTED DATA FOR PHOENIX II

Plasma density and velocity distributions, single particle behaviour and detector efficiencies

G. KUO-PETRAVIC
M. PETRAVIC
A. C. RIVIERE
C. A. STEED
D. R. SWEETMAN

Culham Laboratory
Abingdon Berkshire

1967

Available from H. M. Stationery Office
THREE SHILLINGS AND SIXPENCE NET

U.D.C.
533.93
621.039.624

COMPUTED DATA FOR PHOENIX II: PLASMA DENSITY AND VELOCITY DISTRIBUTIONS, SINGLE PARTICLE BEHAVIOUR AND DETECTOR EFFICIENCIES

by

G. KUO-PETRAVIC
M. PETRAVIC
A.C. RIVIERE
C.A. STEED
D.R. SWEETMAN

A B S T R A C T

The advent of complex field configurations to produce magnetic wells has made desirable a simple method of describing the plasma distribution. One such method is described which essentially gives the plasma distribution in terms of the axial adiabatic invariant (J) and the precessional drift surface described by the radius of a flux tube.

Plasma distributions in this two dimensional space are plotted for typical PHOENIX II injection conditions and, using similar computer programs, the efficiency of neutral particle emission detectors is calculated. Other properties such as the average anisotropy and precessional drift frequency have been computed.

U.K.A.E.A. Research Group,
Culham Laboratory,
Abingdon,
Berks.

September, 1967 (C18/MEJ)

CONTENTS

1. INTRODUCTION

The magnetic field configuration of PHOENIX II is that of a simple mirror with a quadrupole cusp field superimposed to produce a magnetic well. The plasma is formed by the injection of a mono-energetic beam of particles and has a rather complicated shape (Fig.1). This report describes some of the computer calculations which have been carried out on the properties of the plasma and of the containing field.

In particular in a magnetic field of such complex shape it is clearly useful to have a simple two dimensional plot of the plasma distributions. On the assumption of adiabatic invariance it is possible to completely define the plasma in terms of the three invariants $M = E_\perp/B$, $J = \oint p_\parallel ds$ and a flux invariant which may loosely be described by the radius of a flux tube. This is a familiar way of describing the distribution of particles in the earth's magnetic field but has not been used extensively otherwise.

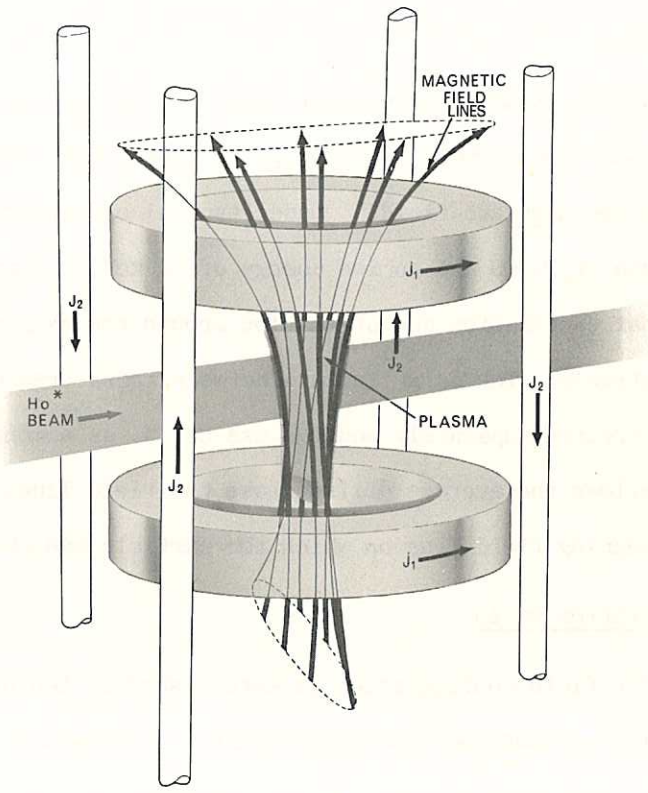

Fig. 1 Magnetic field configuration of PHOENIX II (CLM-R76)

On the assumption that the energy of the injected particle remains fixed, the distribution in M becomes redundant and the plasma may be defined by contoured plots in two dimensional space. This technique though discussed here for the specific case of the PHOENIX II experiment may have a quite general application in toroidal as well as mirror geometry.

Other properties of the plasma such as precessional drift rates and anisotropy distributions may be calculated in the course of these computations.

2. THE DRIFT BEHAVIOUR OF SINGLE PARTICLES IN THE PLASMA

Adiabatic Invariants

PHOENIX II is a mirror machine and as such it relies on the adiabatic motion of individual particles for containment. This means that the magnetic moment of an orbiting particle must be a constant of its motion. Although non-adiabatic effects may occur in certain regions of the field for large orbit sizes, in the following calculations both the zero order magnetic moment $M = \frac{\frac{1}{2}mv_\perp^2}{B}$ (where $v_\perp$ is the component of the particle velocity perpendicular to the magnetic field) and the energy $U = \frac{1}{2}mv^2$ are assumed to be constant.

The zero order longitudinal invariant $J = \oint p_{||} ds$ along a field line is also invoked in the calculations where $p_{||} = mv_{||}$, $v_{||}$ being the component of the particle velocity parallel to the magnetic field. Under typical operating conditions such as a central field strength of 20 kG and an ion energy of 20 keV, the frequencies for cyclotron motion, longitudinal oscillation and precession around the axis are of the order of 30, 2 and 0·12 MHz respectively. The large factors between these frequencies allow the three types of motion to be treated separately and the use of J as a constant of motion is justified. This in turn allows the average drift across the field lines to be calculated by moving to that neighbouring field line on which the particle has the same value of J.

Compensation Ratio

The field configuration is established by two principal coil systems - the simple mirror coils and the quadrupole coils. These are known as the Lorentz coils and the Ioffe coils respectively. It is convenient to define a compensation ratio $C_r = \text{const} \times \left(\frac{\text{current in Ioffe coils}}{\text{current in Lorentz coils}}\right)$. With zero current in the Ioffe coils ($C_r = 0$) the radial gradient $\frac{\partial |B|}{\partial r}$ is negative for all radii. As the current in the Ioffe coils is increased $\left|\frac{\partial |B|}{\partial r}\right|$ is reduced until for small radii $\frac{\partial |B|}{\partial r} = 0$ and the negative radial gradient of the simple mirror is just compensated by the positive gradient of the quadrupole field. At this point we set $C_r = 1$, so that for $C_r < 1$ there is no magnetic well and for $C_r > 1$ a well exists. All the present calculations were carried out for the standard condition $C_r = 1{\cdot}5$.

Drift Surfaces

Some studies of the drift motion in a magnetic well have been published previously[1]. These show that some particles precess about the axis of the field and others precess about a point off the axis. In a quadrupole field there are four such off axis points but in

PHOENIX II particles drifting about these points intersect the vacuum walls and are lost. Thus only those particles which precess about the axis form the plasma. A particle with a given U, M and J traces out a unique drift surface[2]. In general the drift surface will intersect the median plane at all azimuths; but for particles with $J \to 0$ this is not so, the surface then only intersects the median plane at each of the azimuths which lie midway between i.e. at $\pi/4$ to the cusp planes. This is simply because the minimum in $|B|$ on a field line does not always occur at the median plane. We define a reference azimuth to be a line in the median plane which passes through the origin and which lies at $\pi/4$ to the cusp planes. The radius R at which the drift surface intersects the reference azimuth and the value of J then suffice to define completely the behaviour of any particle in the plasma. The velocity ratio $VR = \left|\frac{v_{\parallel}}{v_{\perp}}\right|$ defined at the point where the particle passes the reference azimuth is a more understandable physical quantity than J and for this reason we have chosen to define each particle by the quantities R and VR rather than R and J.

Drift Behaviour of Single Particles

Before considering the plasma distributions it is of interest to obtain a picture of the average drift behaviour in PHOENIX II of selected particles in the plasma. To do this, particles were started at the reference azimuth with values of R and VR corresponding to a mesh of points on the R, VR plane. Their average drift was calculated by following the contour of constant J, M and U on the median plane[3] until one octant was completed. Various possibilities occurred. For the acceptable contained particles the drift path intersected both sides of the octant in a single path. For other particles the drift path returned to the azimuth, thus intersecting it twice, or it left the system through the outer limit indicating a collision with the vacuum walls. For the accepted particles whose drift paths encircled the axis both directions of drift motion could occur. This direction could be deduced from $\frac{\partial J}{\partial r}$, as shown in eq.(4) later. For those particles completely contained within the well the average radial gradient is positive and drift occurs in the flute stable direction. Other

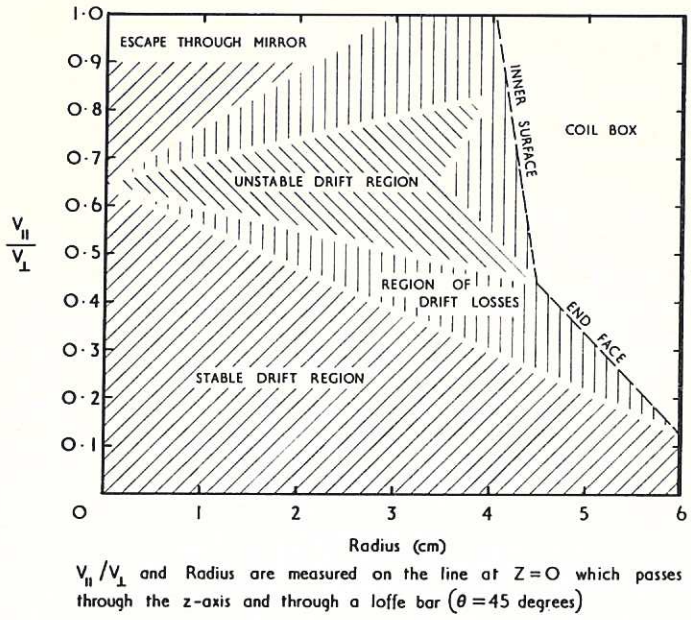

$V_{\parallel}/V_{\perp}$ and Radius are measured on the line at Z = O which passes through the z-axis and through a Ioffe bar (θ = 45 degrees)

Fig. 2 (CLM-R76)
Summary of drift behaviour

particles with sufficiently large VR spend some time outside the well in regions of negative radial gradient and they drift in the opposite direction. Between these two extremes the drift motion is slow and undefined, and leads to losses to the walls. A summary of the drift behaviour on the R, VR plane for $C_r = 1{\cdot}5$ is shown in Fig.2. Although a value of VR of 0·95 is required for an axial particle to escape through the mirror drift losses to the walls will occur at VR = 0·65. This value becomes even smaller for finite values of R. Thus there is a drift loss cone which limits the maximum value of VR in the plasma.

Precessional Drift Frequencies

The drift velocity which is of interest for the study of drift waves can be obtained from $\left(\frac{\partial J}{\partial r}\right)_{\alpha MU}$ by using the results of J.B. Taylor[4]. If one writes

$$B = \nabla\alpha \times \nabla\beta \ , \qquad \ldots (1)$$

then clearly α,β are constant along a field line so that α,β can be regarded as the coordinates of that field line. More specifically, if we consider any surface S cut by field lines and draw on this surface the lines of α = constant, β = constant, then these lines form a coordinate grid on which the lines of force are located by the α,β value of their intersection with S. The drift motion in the plane defining α and β is given[4] by,

$$\dot{\alpha} = -\frac{c}{e}\frac{\partial U}{\partial \beta}(M,\ J,\ \alpha,\ \beta)$$

$$\dot{\beta} = +\frac{c}{e}\frac{\partial U}{\partial \alpha}(M,\ J,\ \alpha,\ \beta)$$

$$\dot{J} = 0$$

Before being able to obtain real velocities from $\dot{\alpha}$ and $\dot{\beta}$ we need to know how to transform from the α,β to the x,y system. The scale of the coordinate α,β can be chosen so that the flux through any part ΔS at the surface S is numerically equal to $\iint_{\Delta S} d\alpha d\beta$. We choose the surface S to be the plane z = 0. We can write

$$\iint B_z dxdy = \iint d\alpha d\beta \ , \qquad \ldots (2)$$

but we are still free to choose the precise form of the transformation. For simplicity we choose $y = \beta$ everywhere, then immediately

$$\frac{\partial y}{\partial \beta} = 1, \quad \frac{\partial y}{\partial \alpha} = 0 \ ,$$

also (2) becomes

$$\alpha = \int_0^x B_z(x,y)\, dx = I(x,y) \ . \qquad \ldots (3)$$

Differentiating (3) with respect to α we find

$$\frac{\partial x}{\partial \alpha} = \frac{1}{B_z} .$$

Differentiating (3) with respect to β we find

$$\frac{\partial x}{\partial \beta} = \frac{1}{B_z} \frac{\partial I(x,y)}{\partial y} .$$

The drift velocity in the plane $z = 0$ is given by

$$v^2_{Drift} = \dot{x}^2 + \dot{y}^2 ,$$

$$= \left(\frac{\partial x}{\partial \alpha} \dot{\alpha} + \frac{\partial x}{\partial \beta} \dot{\beta}\right)^2 + \left(\frac{\partial y}{\partial \alpha} \dot{\alpha} + \frac{\partial y}{\partial \beta} \dot{\beta}\right)^2 ,$$

$$= \frac{1}{B_z^2} \left(\dot{\alpha} - \frac{\partial I(x,y)}{\partial y} \dot{\beta}\right)^2 + \dot{\beta}^2 .$$

If we restrict our attention to the line $x = 0$ and arrange for this line to lie on a reference azimuth then by symmetry we can say $\dot{\beta} = \dot{y} = 0$ and therefore

$$v_{Drift} = \frac{1}{B_z} \dot{\alpha} = - \frac{c}{e} \frac{1}{B_z} \frac{U_o}{U} \left(\frac{\partial U}{\partial y}\right)_{\alpha,M,J} ,$$

where U_o/U is the relationship between the energy units and the units used in the computer calculations. Now since we normally calculate J for constant U and M, the gradient $\left(\frac{\partial U}{\partial y}\right)_{\alpha,M,J}$ is more usefully written in terms of $\left(\frac{\partial J}{\partial y}\right)_{\alpha,M,U}$. U is a function of α, β, M and J so that

$$dU = \left(\frac{\partial U}{\partial \alpha}\right)_{\beta,M,J} d\alpha + \left(\frac{\partial U}{\partial \beta}\right)_{\alpha,M,J} d\beta + \left(\frac{\partial U}{\partial M}\right)_{\alpha,\beta,J} dM + \left(\frac{\partial U}{\partial J}\right)_{\alpha,\beta,M} dJ .$$

For α, M and U constant

$$\left(\frac{\partial U}{\partial \beta}\right)_{\alpha,M,J} = - \left(\frac{\partial U}{\partial J}\right)_{\alpha,\beta,M} \cdot \left(\frac{\partial J}{\partial \beta}\right)_{\alpha,M,U} .$$

We also know[2] that $\left(\frac{\partial J}{\partial U}\right)_{\alpha,\beta,M} = T$, where T is the period of the longitudinal oscillation.

$$\therefore \left(\frac{\partial U}{\partial \beta}\right)_{\alpha,M,J} = \left(\frac{\partial U}{\partial y}\right)_{\alpha,M,J} = - \frac{1}{T} \cdot \left(\frac{\partial J}{\partial y}\right)_{\alpha,M,U}$$

$$\therefore v_{Drift} = \frac{c}{e} \frac{U_o}{U} \frac{1}{B_z} \frac{1}{T} \left(\frac{\partial J}{\partial y}\right)_{\alpha,M,U} . \qquad \ldots (4)$$

We now assume that the drift contours are circular, which is a good approximation in the region of interest, and that v_{Drift} is independent of azimuth to obtain the precessional drift frequency

$$f_{Drift} = \frac{2\pi R}{v_{Drift}} \quad .$$

A plot of lines of constant frequency obtained in this way is shown in Fig.3 for $C_r = 1{\cdot}5$.

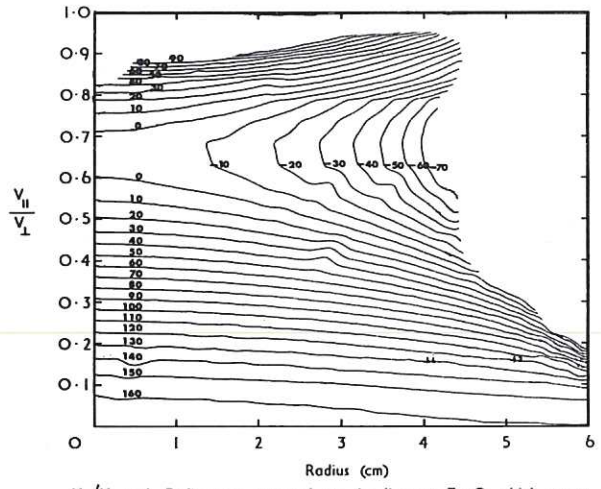

Fig.3 (CLM-R76)
Map of presessional drift frequencies in kH_z. $C_R = 1.5$, $B_o = 17$ kG, $H^o = 20$ keV.

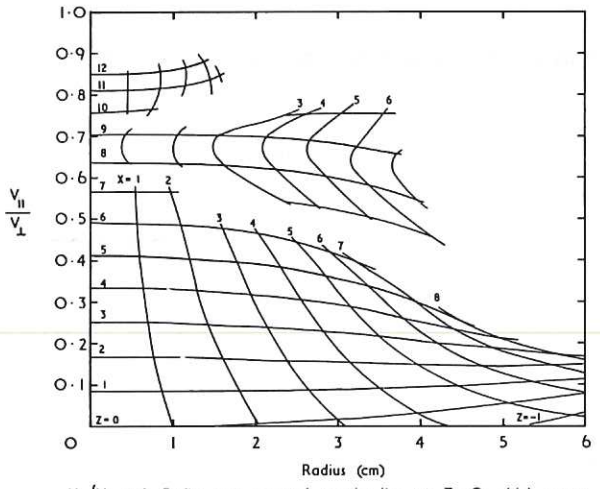

Fig.4 (CLM-R76)
Mapping of mirror points in Y = 0 (cusp) plane for positive values of z. $C_R = 1.5$.

Mapping of Mirror Points

It is also of interest to consider the real coordinates of the mirror points for particles with given values of R and VR. Since there is no azimuthal symmetry the plane on which these points lie must be defined. An example is shown in Fig.4 for mirror points in a cusp plane mapped onto the R, VR plane. Only half of this plane is shown and the sign of the real coordinate z depends on which cusp plane is considered. Its main use is in determining what particles are lost on a metal scraper probe inserted into the plasma region.

3. THE INJECTED PLASMA DENSITY AND VELOCITY DISTRIBUTIONS

The Guiding Centre Distribution of all Particles

The plasma in PHOENIX II is produced by first accelerating a beam of ions to the required energy, passing these through a gas cell so that most of the ions become neutral by electron capture and then passing the beam of fast atoms through the magnetic field. In the field some of the atoms are ionized either by collisions or by Lorentz ionization and are then trapped in the system to form the plasma. Each particle can be described by the

appropriate R and VR values and the distribution of all the particles on the $(R, VR)_{U = \text{constant}}$ plane will completely describe the plasma.

To calculate this distribution, the injected beam is synthesized from a set of 9 × 9 parallel trajectories separated apart by 1 cm. These trajectories are weighted by the beam profile which is assumed to be solely determined by a uniformly illuminated neutralizer cell and an intervening aperture. Atoms are assumed to be ionized at 0·5 cm intervals along these line trajectories, and it is necessary to calculate the Lorentz trapping probability at each point. For the 0^{o} injection case, where the beam was injected normal to the field axis, the ionization probability was taken to be uniform. Since the radius of the interesting trapping region is quite small this corresponds quite well to both gas trapping and Lorentz trapping[5]. For the 15^{o} injection case, where the beam was at 75^{o} to the field axis the Lorentz trapping probability was calculated by taking ΔE (the electrical field difference between neighbouring points) and weighting it by a classical Lorentz trapping probability curve of $\frac{dN(E)}{dE}$ vs E. That is the trapping probability used was $\sim \frac{dN(E)}{dE} \Delta E$. At each point of ionization the guiding centre for the ion and its magnetic moment $M = E_{\perp}/|B|$ are calculated. Those ions whose value of M is so small that they escape through the mirrors, obviously make no contribution. The value of the longitudinal invariant J is calculated by integration along the field line which passes through the guiding centre position. The precessional drift behaviour of the ion is then determined by the surface of constant M and J which contains the starting point. Because of the symmetry properties of the quadrupole field, the surface need be followed for one octant only. If the drift surface contains the axis and nowhere touches the walls of the system, the drift is acceptable. For all other cases the ion is assumed to be not contained. The radius R at which the drift surface intersects the reference azimuth and the value of the ratio $VR = |v_{\parallel}/v_{\perp}|$ at that point are then recorded. Values for R and VR are calculated for ions trapped at each point on each injection line and the number of guiding centres, Ngc, which lie in each element of area in the R, VR plane is computed.

As the total number of points calculated was not sufficient to give a smooth overall picture, an interpolation programme[3] was used to increase the number of points in each cell; the cell size was 0·025 in VR and 0·125 cm in R. By drawing contours of constant Ngc on the R, VR diagram the distribution of particles can readily be seen. This is illustrated by the three examples in Fig.5(a), (b) and (c). Conditions for each of these examples were such that the orbit radius at the centre was 1·14 cm. This

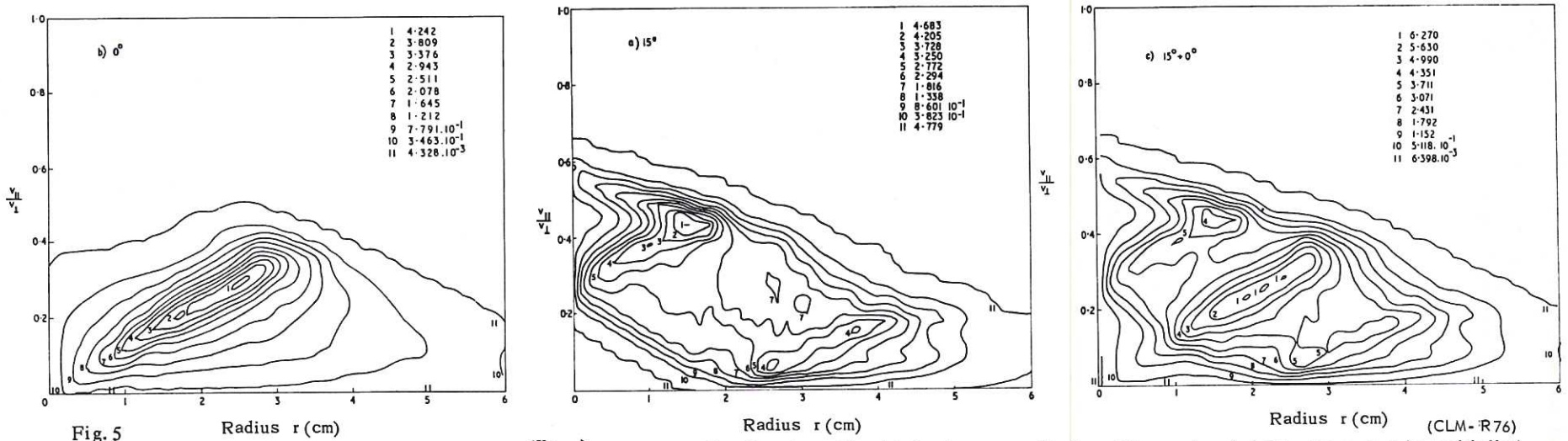

Fig. 5 Guiding centre 'density' contours for $z = 0$ in the $\left(\frac{v_{\parallel}}{v_{\perp}}, r\right)$ plane for 0°, 15°, and combined injection respectively. The contour heights shown may be multiplied by 5×10^{-5} to obtain 'density' per unit area of $\left(\frac{v_{\parallel}}{v_{\perp}}, r\right)$ diagram where 'density' is fraction of total beam possessing an excited state population distribution = $1/n^3$ (trapped at 17.3 kG central field 20 keV energy)

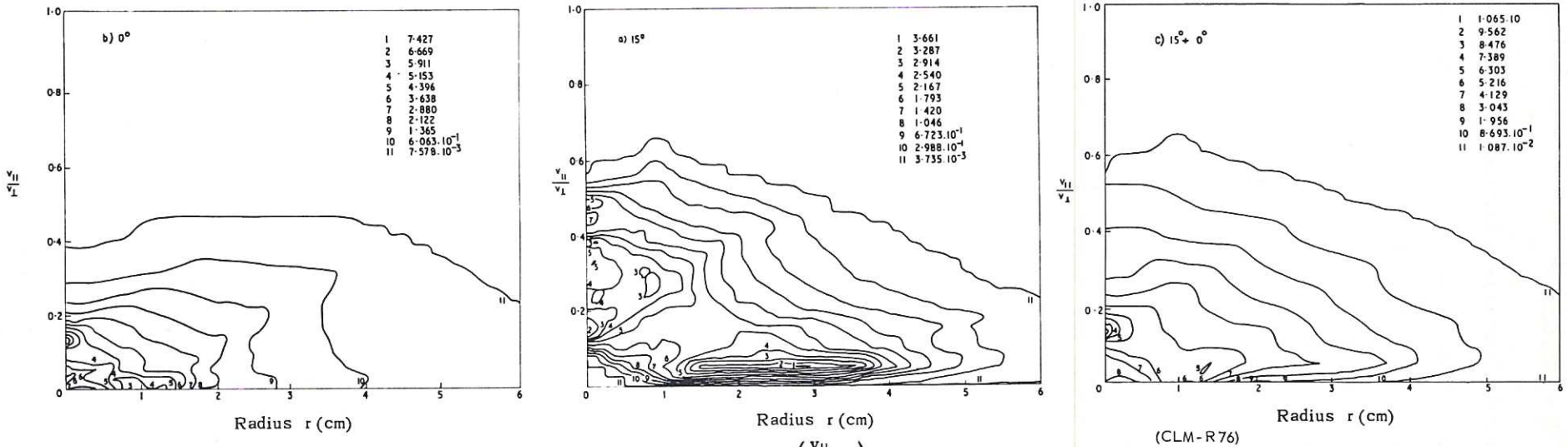

Fig. 6 Real density contours for $z = 0$ in the $\left(\frac{v_{\parallel}}{v_{\perp}}, r\right)$ plane for 0°, 15°, and combined injection respectively. The units shown may be inferred from the text and the caption for Fig. 5.

corresponds to an ion energy of 20 keV and a field strength of 17·8 kG. The compensation ratio was 1·5. Fig.5(a) shows the contour for 0^{o} injection and Fig.5(b) the 15^{o} injection case. In Fig.5(c) the beams of 5(a) and 5(b) were assumed to be injected simultaneously.

The Ion Density and Velocity Distributions

The matrix Ngc (R, VR) describes the distribution of all the particles in terms of the positions of their guiding centres. To obtain the actual density at any given point account must be taken of finite orbit size, velocity along the field line and precession about the axis. The corrections for finite Larmor radius and for the spread around the axis due to precessional drift are calculated for each point taking into account the value of the Larmor radius (given by VR) and R at that point.

Let us call this new matrix NR (R, VR); now if we keep R fixed and plot NR aginst VR, we are effectively plotting a function

$$\hat{f}\left(\frac{v_{o\parallel}}{v_{o\perp}}\right) = \frac{dN(z = 0)}{d\left(\frac{v_{o\parallel}}{v_{o\perp}}\right)} \quad .$$

This is not the correct velocity distribution function defined as $f\left(\frac{V_{\parallel}}{V_{\perp}}, Z\right)$ for a general case since the fraction of a particle's total cycle that the particle spends between Z and Z + dZ must be calculated. This will of course depend on $\frac{V_{\parallel}}{V_{\perp}}$, in other words, on the turning point. It may be shown that if $B \simeq (1 + 2\alpha Z^2) B_o$

$$\frac{dt}{dz} \cdot \frac{1}{\tau} = \frac{1}{2\pi} \frac{1}{(z_n^2 - z^2)^{\frac{1}{2}}} = \frac{\sqrt{2\alpha}}{2\pi \left(\left(\frac{v_{o\parallel}}{v_{o\perp}}\right)^2 - 2\alpha z^2\right)^{\frac{1}{2}}}$$

where τ is the period of longitudinal oscillation along a field line. We require

$$f\left(\frac{v_{\parallel}}{v_{\perp}}, z = 0\right) \equiv f\left(\frac{v_{o\parallel}}{v_{o\perp}}\right)$$

$$= \hat{f} \times \frac{1}{2\pi} \frac{\sqrt{2\alpha}}{\left(\frac{v_{o\parallel}}{v_{o\perp}}\right)}$$

where $2\alpha = 0{\cdot}0073\ cm^{-2}$ for PHOENIX II. Once $f\left(\frac{v_{o\parallel}}{v_{o\perp}}, 0\right)$ is obtained, a new set of contours of f can be drawn (Fig.6). Figs.7a-f show $f\left(\frac{v_{o\parallel}}{v_{o\perp}}, 0\right)$ against $\frac{v_{o\parallel}}{v_{o\perp}}$ for different radii. The eight curves in Fig.7a correspond to the values of R between 0 and 1 cm, those in Fig.7b between 1 cm and 2 cm, and so on. The area under each curve is proportional to density. Figs.8 and 9 show the corresponding curves for 15^{o} and combined injection respectively. It is also interesting to calculate the velocity distribution

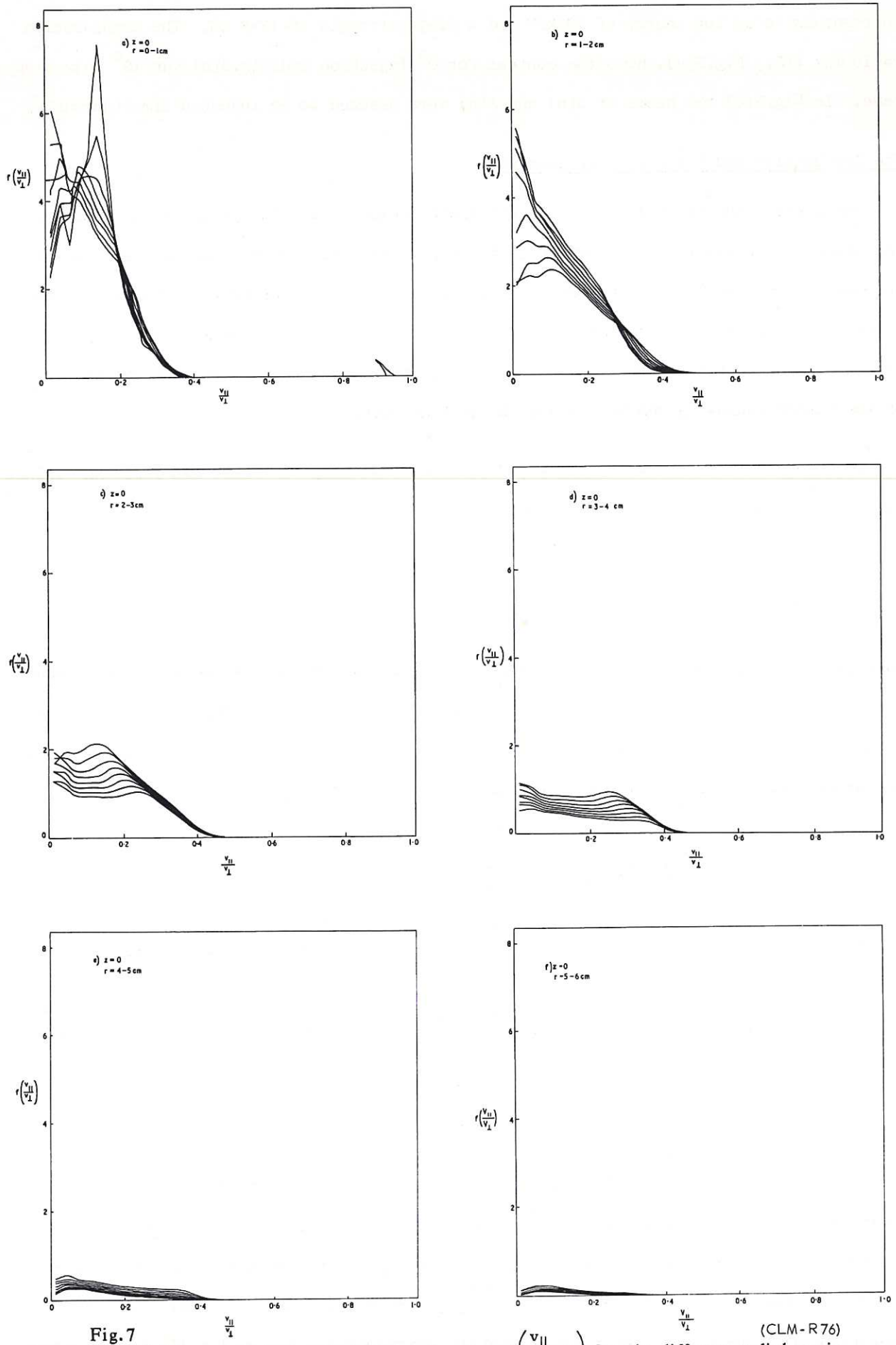

Fig. 7 (CLM-R76)
The 0° injection velocity distribution functions $f\left(\frac{v_{\parallel}}{v_{\perp}}, o\right)$ for six different radial positions r. The units shown may be inferred from the transformations described in the text and the caption for Fig. 5.

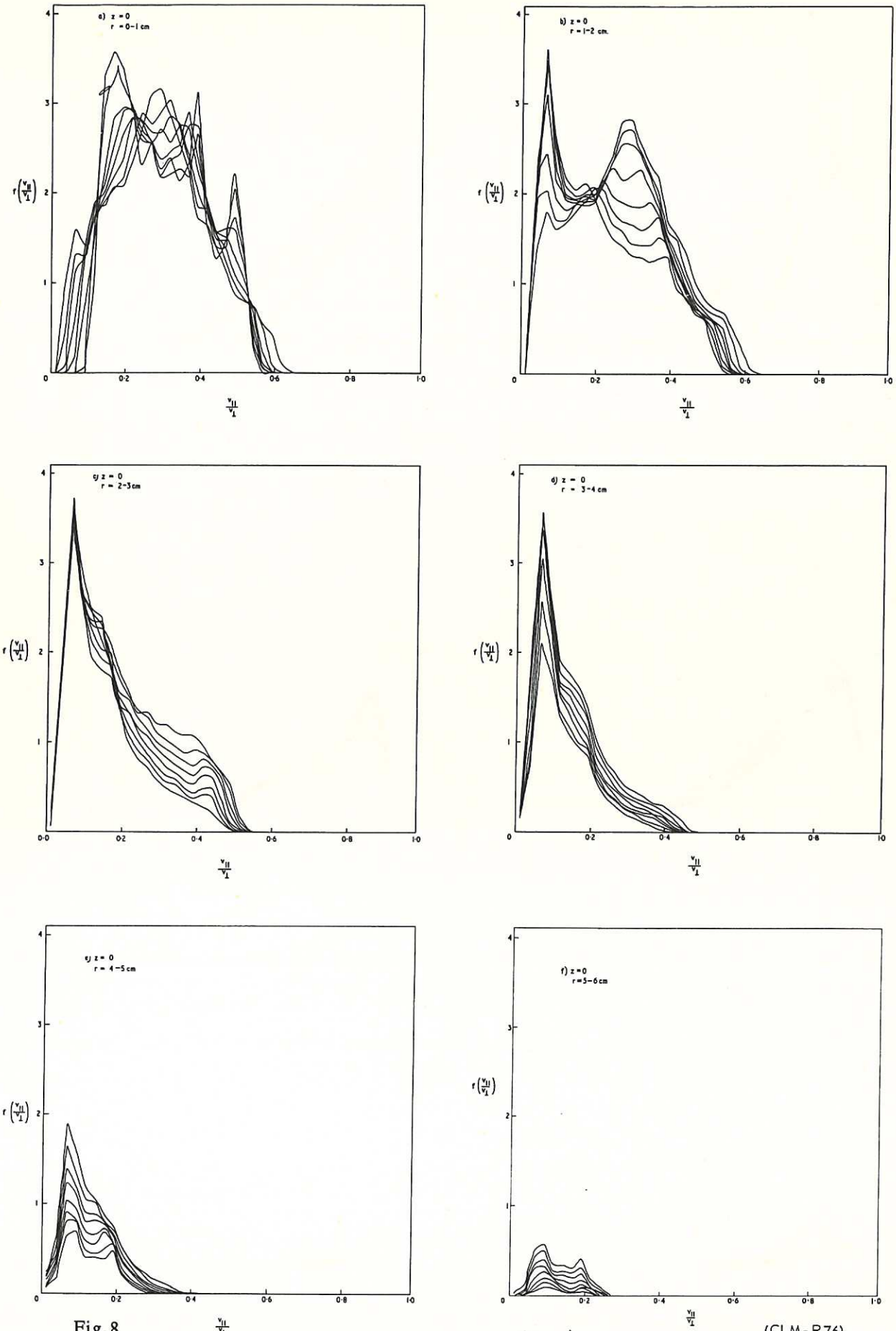

Fig. 8 (CLM-R76)

The 15° injection velocity distribution functions $f\left(\frac{v_{\parallel}}{v_{\perp}}, o\right)$ for six different radial positions r. The units are as for Fig. 7.

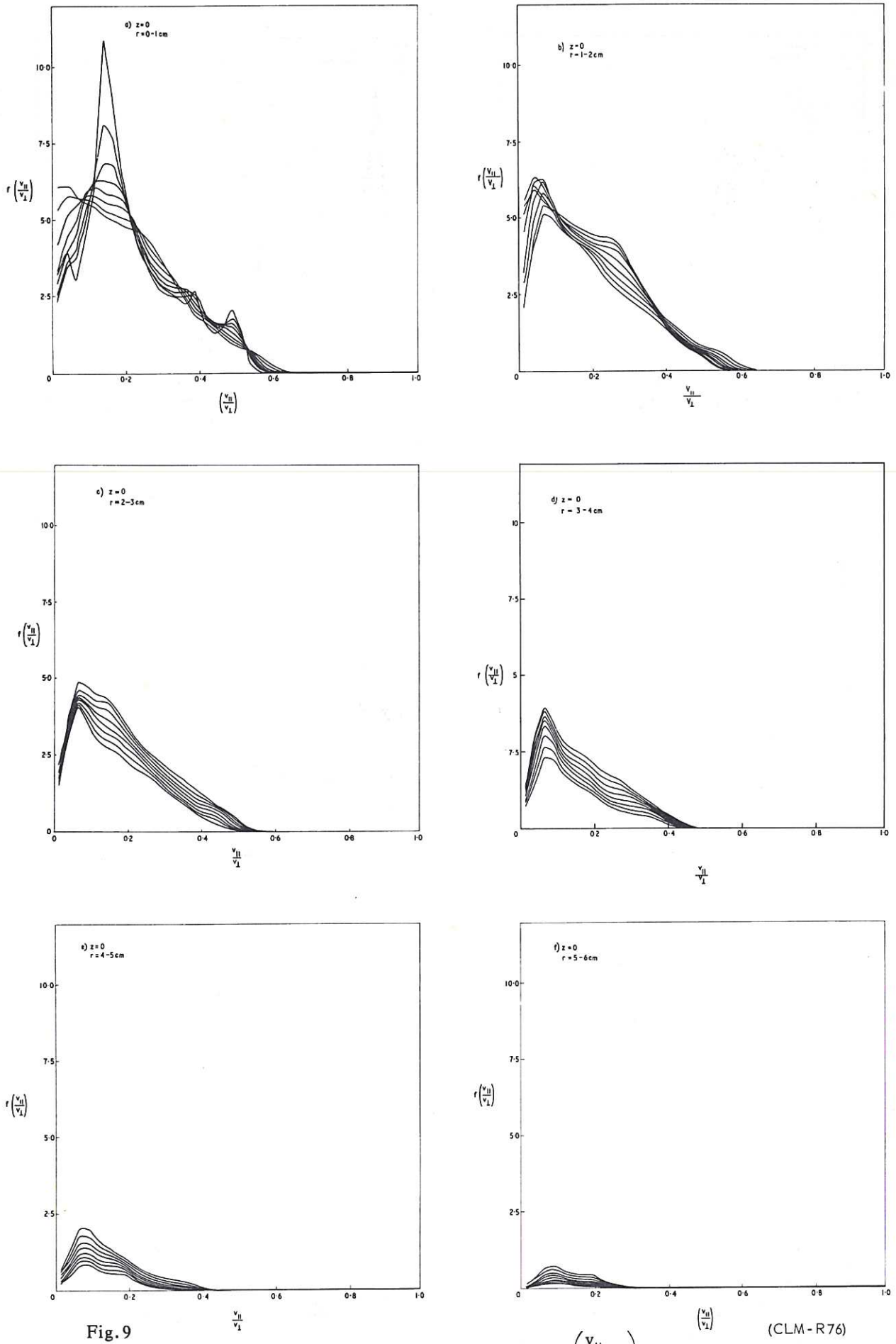

Fig. 9 (CLM-R76)

The combined injection velocity distribution functions $f\left(\frac{v_{||}}{v_\perp}, o\right)$ for six different radial positions r. The units are as for Fig. 7.

function and density at various values of $Z = 1$ cm, 2 cm, ... 6 cm. In order to transform $f\left(\frac{V_{o\parallel}}{V_{o\perp}}, z = 0\right)$ to $f\left(\frac{V_\parallel}{V_\perp}, z\right)$ the following relation is used.

The value of anisotropy $\frac{V_{o\parallel}}{V_{o\perp}}$ is transformed to a value of $\frac{V_\parallel}{V_\perp}$ at z by

$$\frac{V_\parallel}{V_\perp} = \left(\frac{\frac{V_{o\parallel}}{V_{o\perp}} - 2\alpha z^2}{1 + 2\alpha z^2} \right)^{\frac{1}{2}} . \qquad \ldots (5)$$

At this new value of $\frac{V_\parallel}{V_\perp}$, the number per unit interval in $\left(\frac{V_\parallel}{V_\perp}\right)$, namely $f\left(\frac{V_\parallel}{V_\perp}, z\right)$, can be found by the number per unit interval at $z = 0$ multiplied by

$$\frac{d\left(\frac{V_{o\parallel}}{V_{o\perp}}\right)}{d\left(\frac{V_\parallel}{V_\perp}\right)}$$ which can be obtained from eq.(5).

Therefore

$$f\left(\frac{V_\parallel}{V_\perp}, z\right) = \hat{f} \; \frac{\sqrt{2\alpha}}{2\pi\left(\left(\frac{V_{o\parallel}}{V_{o\perp}}\right)^2 - 2\alpha z^2\right)^{\frac{1}{2}}} \times \frac{\sqrt{1 + 2\alpha z^2}}{1} \times \frac{\sqrt{\left(\frac{V_{o\parallel}}{V_{o\perp}}\right)^2 - 2\alpha z^2}}{\sqrt{\left(\frac{V_{o\parallel}}{V_{o\perp}}\right)^2}}$$

$$= \hat{f} \times \frac{\sqrt{2\alpha}}{2\pi} \; \frac{\sqrt{1 + 2\alpha z^2}}{\left(\frac{V_{o\parallel}}{V_{o\perp}}\right)} = f\left(\frac{V_{o\parallel}}{V_{o\perp}}, z = 0\right) \times \sqrt{1 + 2\alpha z^2} \qquad \ldots (6)$$

In the computation, average values of f at $z = 0$ over 1 cm intervals are used. The transformation is then performed by fixing intervals in $\frac{V_\parallel}{V_\perp}$ at $z = 1, 2, 3, 4, 5, 6$ cm and calculate with the aid of equations (5) and (6).

Fig.10 shows the results for 0^o injection. The first seven curves show f at $z = 0, 1, 2, 3, 4, 5$ and 6 for the radial range 0 - 1 cm. The second seven curves show the similar results for the radial range 1 - 2 cm, and so on up to radial range 5 - 6 cm.

Figs.11 and 12 show the results for 15^o and combined injection. The area under these curves is proportional to density in each case.

It is also possible to find the average anisotropy for all particles on a field line, i.e. average over oscillations up and down the mirror. If we define the average anisotropy to be $\frac{\langle E_\parallel \rangle}{\langle E_\perp \rangle}$, for each particle, this is given by

$$\frac{\langle E_\parallel \rangle}{\langle E_\perp \rangle} = \frac{\left(\frac{V_{o\parallel}}{V_{o\perp}}\right)^2}{2 + \left(\frac{V_{o\parallel}}{V_{o\perp}}\right)^2} .$$

This has to be weighted by the distribution function f for all particles on a field line.

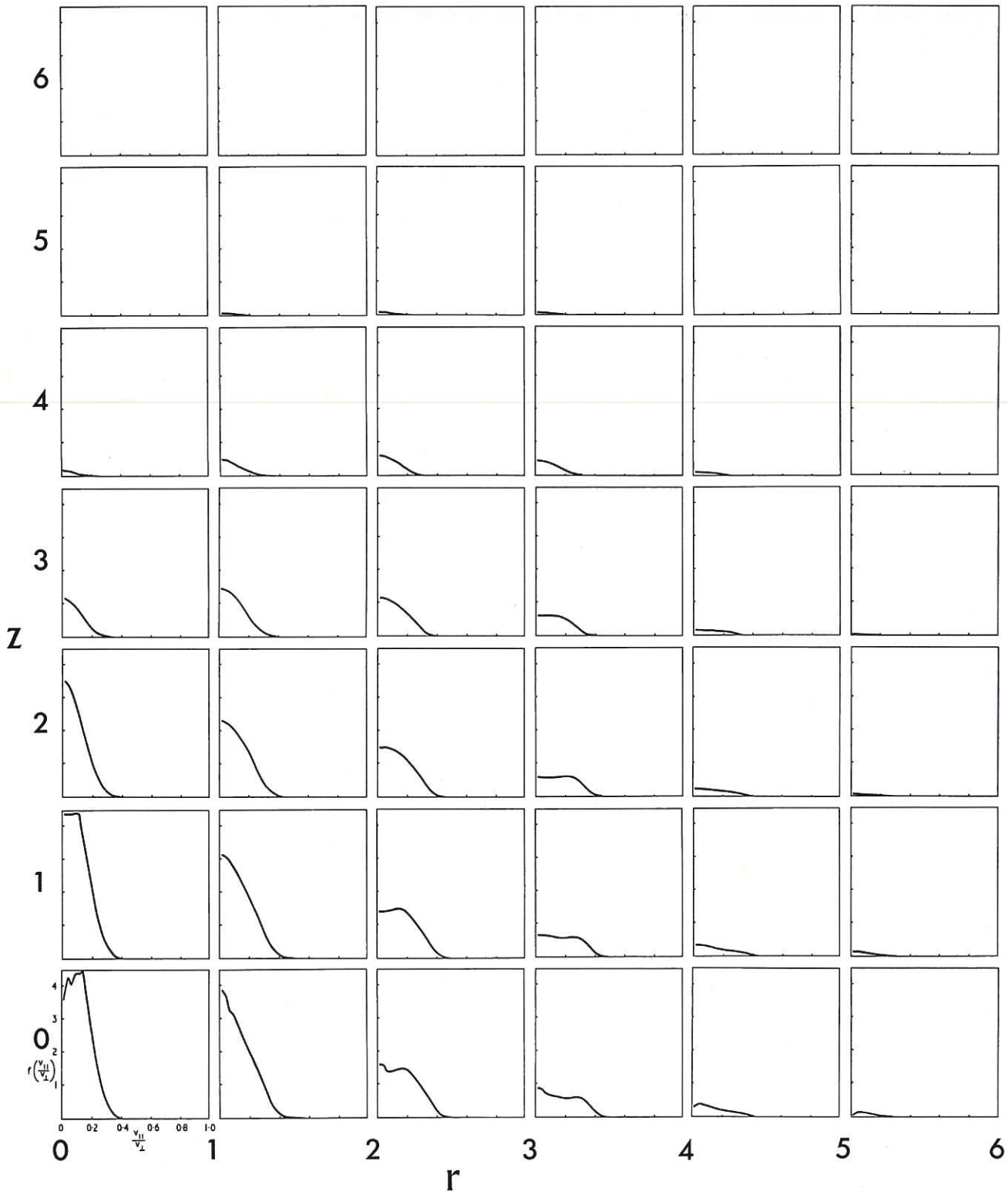

Fig. 10 (CLM-R76)

The 0° injection velocity distribution functions $f\left(\frac{v_{\parallel}}{v_{\perp}}, o\right)$ for different values of radial and axial positions r and z. The units may be inferred from the transformations described in the text and the caption for Fig. 5.

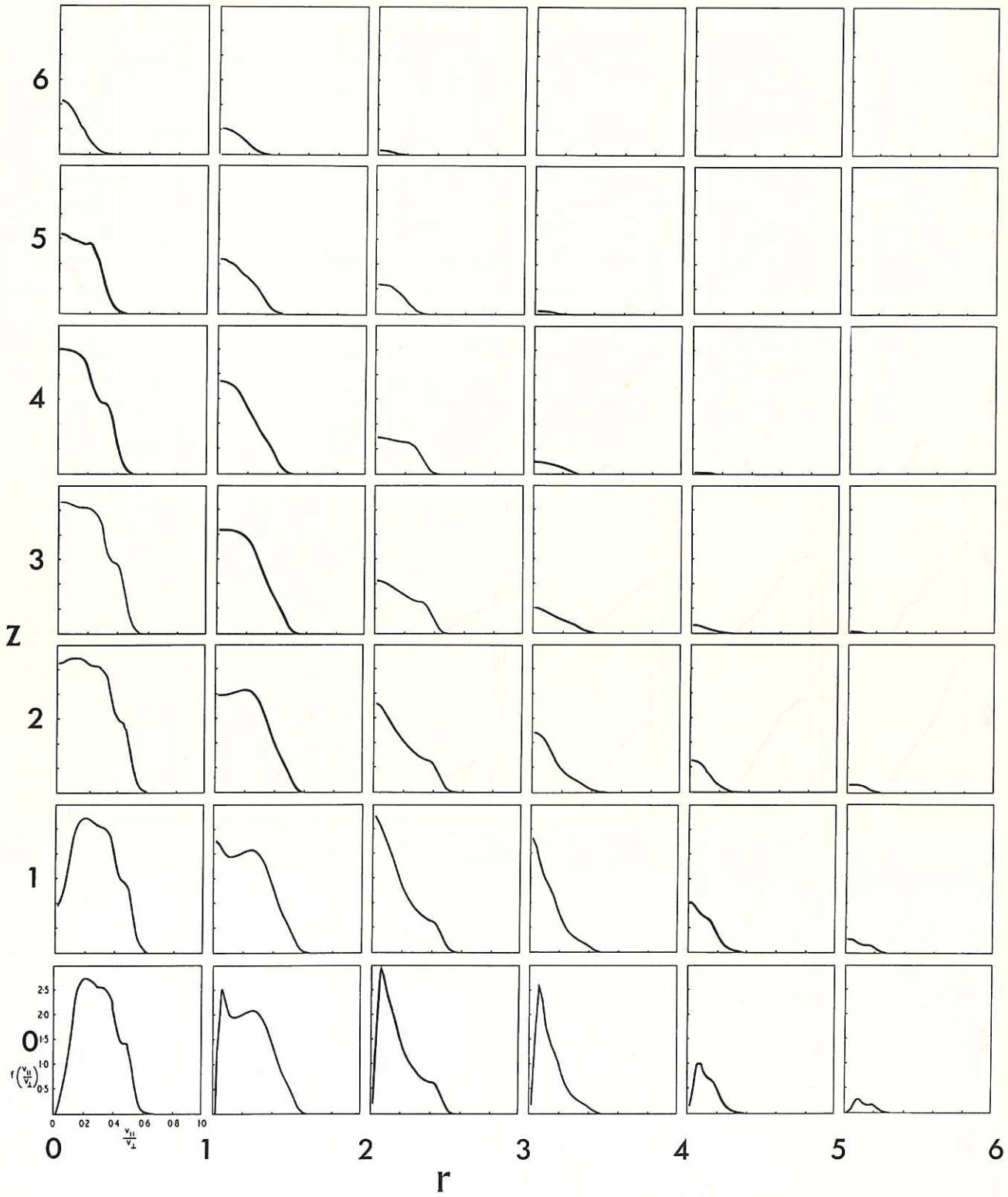

Fig. 11 (CLM-R76)

The 15° injection velocity distribution functions $f\left(\frac{v_{\parallel}}{v_{\perp}}, o\right)$ for different values of radial and axial positions r and z. The units are as for Fig. 10.

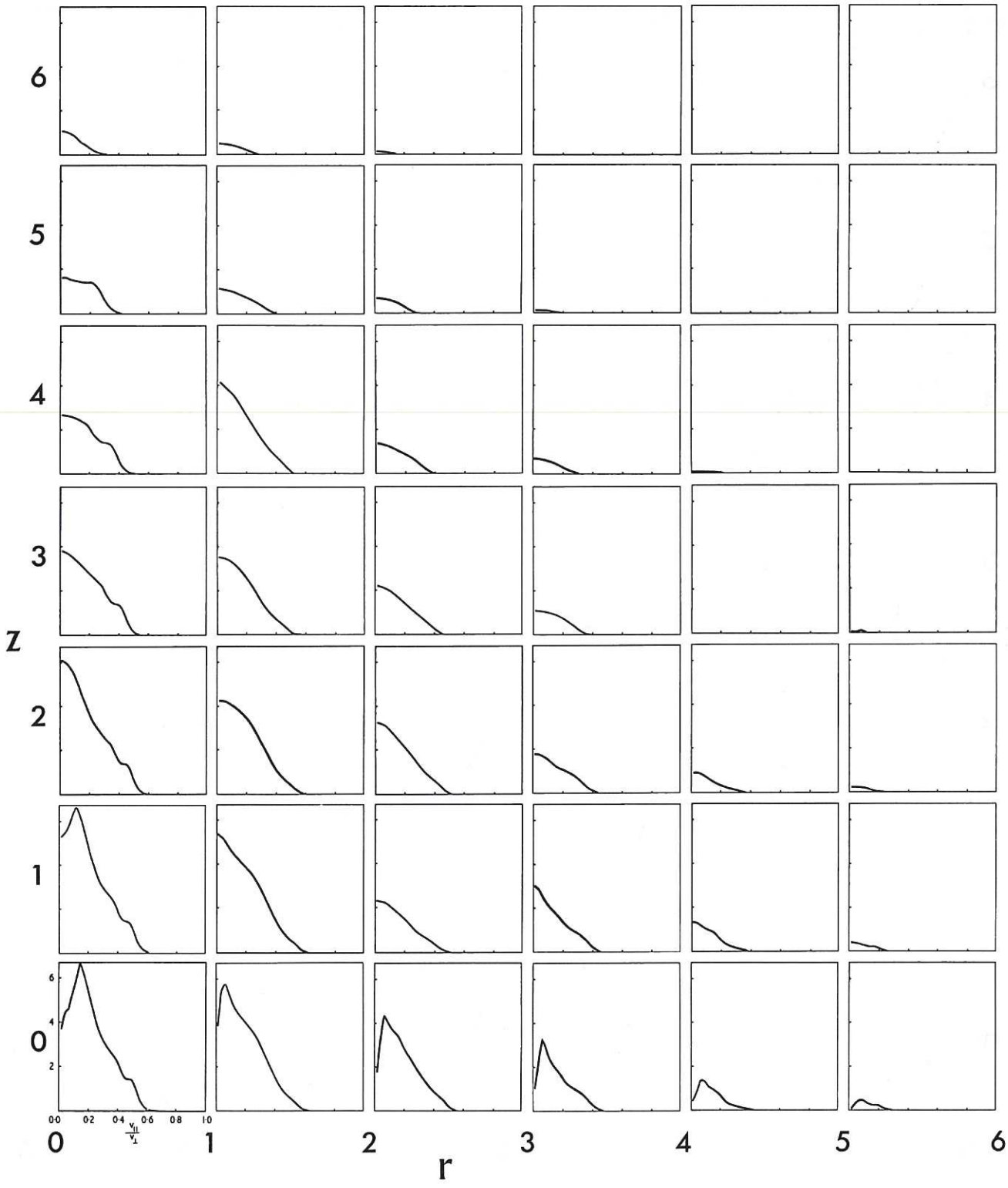

Fig. 12 (CLM-R76)
The combined injection velocity distribution functions $f\left(\frac{v_{\parallel}}{v_{\perp}}, o\right)$ for different values of radial and axial positions r and z. The units are as for Fig. 10.

Therefore

$$\left\langle \frac{\langle E_{\parallel} \rangle}{\langle E_{\perp} \rangle} \right\rangle = \frac{\int \frac{\langle E_{\parallel} \rangle}{\langle E_{\perp} \rangle} \hat{f}\left(\frac{v_{o\parallel}}{v_{o\perp}}\right) d\left(\frac{v_{o\parallel}}{v_{o\perp}}\right)}{\int \hat{f}\left(\frac{v_{o\parallel}}{v_{o\perp}}\right) d\left(\frac{v_{o\parallel}}{v_{o\perp}}\right)}$$

This integration is performed numerically.

Alternatively, one can obtain an analytic solution for $\langle | \frac{v_{\parallel}}{v_{\perp}} | \rangle$, which was not possible for $\langle \frac{E_{\parallel}}{E_{\perp}} \rangle$

$$\langle | \frac{v_{\parallel}}{v_{\perp}} | \rangle = \frac{4}{\tau} \frac{v_{o\parallel}}{v_{o\perp}} \int_0^{\tau/4} \frac{\text{Cos } \omega t \, dt}{\sqrt{1 + \left(\frac{v_{o\parallel}}{v_{o\perp}}\right)^2 \text{Sin}^2 \omega t}}$$

$$= \frac{2}{\pi} \ell n \left(\frac{v_{o\parallel}}{v_{o\perp}} + \sqrt{1 + \left(\frac{v_{o\parallel}}{v_{o\perp}}\right)^2} \right) .$$

Again, weighting by the line distribution function gives

$$\langle\langle | \frac{v_{\parallel}}{v_{\perp}} | \rangle\rangle = \frac{\int \langle | \frac{v_{\parallel}}{v_{\perp}} | \rangle \hat{f}\left(\frac{v_{o\parallel}}{v_{o\perp}}, z = 0\right) d\left(\frac{v_{o\parallel}}{v_{o\perp}}\right)}{\int \hat{f} \, d\left(\frac{v_{o\parallel}}{v_{o\perp}}\right)}$$

Values of these average anisotropies, and densities at various z are tabulated in Tables 1, 2, and 3.

TABLE 1

0^{o} INJECTION RESULTS

$N_o(R) + 2\sum_{z=1}^{6} N_z(R)$ =	169·6	155·6	112·8	60·6	17·7	3·7
6	0·0	0·0	0·0	0·0	0·0	0·0
5	0·0	0·3	0·3	0·3	0·0	0·0
4	0·7	2·9	3·8	2·9	0·6	0·0
Z_{cm} 3	6·7	10·7	9·8	6·1	1·3	0·1
2	22·3	19·9	15·3	7·5	2·1	0·4
1	36·0	28·0	17·7	8·7	3·0	0·9
0	38·2	32·0	18·8	9·5	3·3	0·9
	0 → 1	1 → 2	2 → 3	3 → 4	4 → 5	5 → 6 R cm
$\left(\left\langle \frac{E_{\parallel}}{E_{\perp}} \right\rangle\right)^{1/2}$	0·13	0·15	0·17	0·19	0·16	
$\langle\langle \lvert \frac{v_{\parallel}}{v_{\perp}} \rvert \rangle\rangle$	0·11	0·13	0·15	0·16	0·13	

$$N_z(R) = \int_0^{\infty} f_z\left(\frac{v_{\parallel}}{v_{\perp}}\right) d\left(\frac{v_{\parallel}}{v_{\perp}}\right)$$

Total number trapped = 520

TABLE 2

15^{o} INJECTION RESULTS

$N_o(R) + 2\sum_{z=1}^{6} N_z(R)$ =

Z_{cm}	407·2 N(R)	300·6	167·0	77·8	30·5	6·7
6	6·6	3·7	0·4	0·0	0·0	0·0
5	17·4	10·5	4·7	0·3	0·0	0·0
4	30·8	20·7	8·5	1·9	0·1	0·0
3	39·8	28·9	12·7	4·2	1·0	0·1
2	45·8	33·1	18·8	9·2	4·0	0·9
1	43·2	36·0	25·9	15·5	6·9	1·7
0	39·6	34·8	25·1	15·5	6·5	1·5
r =	0 → 1	1 → 2	2 → 3	3 → 4	4 → 5	5 → 6 R cm
$\left(\frac{\langle E_{\parallel}\rangle}{\langle E_{\perp}\rangle}\right)^{\frac{1}{2}}$	0·24	0·23	0·20	0·15	0·12	
$\langle\langle\lvert\frac{v_{\parallel}}{v_{\perp}}\rvert\rangle\rangle$	0·21	0·20	0·16	0·12	0·10	

$$N_z(R) = \int_0^{\infty} f_z\left(\frac{v_{\parallel}}{v_{\perp}}\right) d\left(\frac{v_{\parallel}}{v_{\perp}}\right)$$

Total number trapped = 989

TABLE 3

COMBINED INJECTION RESULTS

$N_o(R) + 2\sum_{z=1}^{6} N_z(R)$ =

Z_{cm}	576·8	456·2	229·8	158·4	28·2	10·4
6	6·6	3·7	0·4	0·0	0·0	0·0
5	17·5	10·8	4·9	0·6	0·0	0·0
4	31·6	23·6	12·3	4·8	0·7	0·0
3	46·5	39·6	22·4	10·3	2·3	0·2
2	68·1	53·1	34·1	16·7	6·1	1·3
1	79·2	63·9	43·6	24·2	9·9	2·6
0	77·8	66·7	43·9	24·9	9·8	2·4
	0 → 1	1 → 2	2 → 3	3 → 4	4 → 5	5 → 6 R cm
$\left(\frac{\langle E_{\parallel}\rangle}{\langle E_{\perp}\rangle}\right)^{\frac{1}{2}}$	0·22	0·21	0·19	0·17	0.14	
$\langle\langle\lvert\frac{v_{\parallel}}{v_{\perp}}\rvert\rangle\rangle$	0·18	0·17	0·16	0·14	0·11	

$$N_z(R) = \int_0^{\infty} f_z\left(\frac{v_{\parallel}}{v_{\perp}}\right) d\left(\frac{v_{\parallel}}{v_{\perp}}\right)$$

Total number trapped = 1509

It is of interest to consider the distributions and their uses. The distributions of total number (e.g. Fig.5) have the advantage that the total number of particles is conserved if parts of the plasma are redistributed in (R, VR) space. They are also in an appropriate form for comparison with other parameters such as detector efficiency which will be described later.

The distribution of ion density on the median plane shown in Fig.6 gives a picture of the actual ion density distribution in real space and is relevant therefore to plasma trapping and the assessment of density gradients. The velocity distributions of Figs.7 to 22 are of obvious interest for the discussion of stability as are the average anisotropies. For instance, the calculations for injection at 15^{o} have shown that there is an increase of $\left\langle \frac{E_{\parallel}}{E_{\perp}} \right\rangle$ of about a factor two in going from 0^{o} to 15^{o} injection as well as an increase in ion density.

4. THE MAPPING OF PARTICLE DETECTOR FIELDS OF VIEW

For a complete link between observation and prediction it is necessary to know which particles in the plasma will be seen by a given detector and the methods used for calculating this will now be described. The types of detector which are considered see only fast neutral atoms leaving the plasma as the results of the capture of an electron by a fast ion. The electron is captured during a collision with a background gas molecule and the assumption is usually made that the background gas density is uniform. A particle with given R and VR values will spend a fraction of its total time in the field of view of the given detector. This fraction we call the detector efficiency E(R,VR). Contours of constant E(R,VR) can be drawn on the R, VR diagram for each detector and compared with the plasma distribution. Two types of detector have been considered.

Single Particle Crystal Detector with Circular Apertures

The first type of detector consists of either a solid state detector or CsI crystal and photomultiplier arrangement which view the plasma through two circular apertures. The basic question to be answered is whether a particle at the point x, y, z in the plasma with direction cosines ℓ,m,n for its velocity can 'see' through both apertures. Each aperture is defined by its radius, the coordinates of its centre and the direction cosines for the normal to the plane of the aperture. The projection of the particles velocity vector may or may not intersect this plane; if it does, then the distance from the point of intersection to the centre of the aperture must be less than the radius of the aperture. If this is true for both apertures, then the particle can 'see' the detector.

If we define the ability to see by the function $F(\vec{r},\vec{v})$ where $\vec{r},\vec{v}$ are the real coordinates of the particle at any given time, then the efficiency is given by

$$E(R,VR) = \frac{1}{2\pi}\int_0^{2\pi} \frac{1}{\tau_\ell}\oint \frac{1}{2\pi}\int_0^{2\pi} F(\vec{r},\vec{v})\,d\theta\,dt\,d\varphi \ .$$

The first integration is taken over the cyclotron orbit, the second over a complete oscillation along the field line, and the third over a complete precessional drift cycle. To simplify the calculation the precessional drift surface is assumed to intersect the median plane in a circle and the velocity around this circle is assumed to be constant. Also, as previously, the particle is assumed to move on a single field line during one complete longitudinal oscillation. To search the whole R,VR plane would require an immense amount of computer time, especially for a tightly collimated detector. To know where to start, the detector is treated as an injector. An atom coming through the apertures traverses the plasma along a known trajectory. At specific points P along the trajectory, the atom is assumed to be ionized and the appropriate values of R and VR for this point are calculated. The integral for E(R,VR) is then solved in the neighbourhood of the point P. To define the appropriate trajectories coming from the detector the apertures are each divided into four smaller apertures and the sixteen possible pairs treated individually. This was the maximum subdivision for the value of E(R,VR) to be obtained in a reasonable amount of computing time.

The contour plot of E(R,VR) for one detector is shown in Fig.13. This detector viewed the plasma along a reference azimuth and was collimated by two apertures 5 mm in diameter at 20 and 80 cms from the plasma. The presence of two peaks is due to the coarseness of the steps in the calculations and this diagram serves only as a guide to the region of maximum efficiency. The outer contour is drawn at 10^{-3} of the peak value and indicates the limits of the field of view.

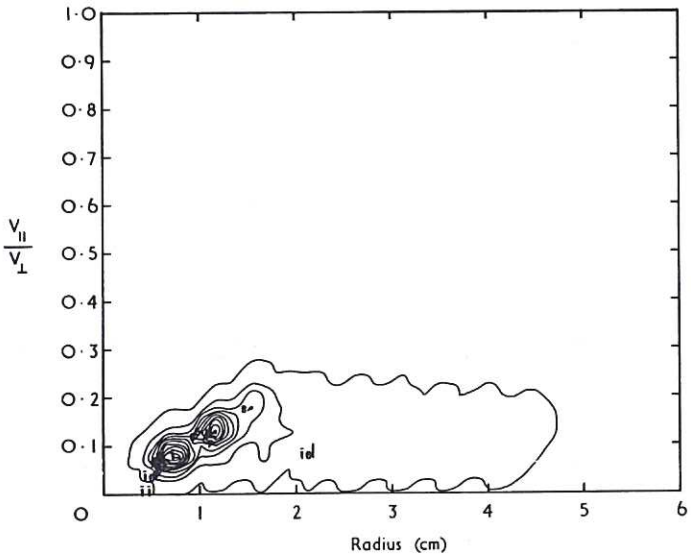

$V_{II}/V_\perp$ and Radius are measured on the line at Z = O which passes through the z-axis and through a Ioffe bar (θ = 45 degrees)

Fig. 13 (CLM-R76)
Detector efficiency map. PM at 45°, z = 0 cm, R_L = 1.14 cm, C_R = 1.5. Radius of aperture (1) = 5 mm; distance from z-axis = 20 cm. Radius of aperture (2) = 5 mm; distance from z-axis = 86 cm.

Total Neutral Emission Detector

The second type of detector consists either of a simple metal plate which registers secondary electron current proportional to the

number of fast atoms hitting it or a plate of phosphor which is viewed by a photomultiplier. No collimation is used in either case so that the idea of inverse injection can no longer be used to advantage. The plate is specified by the coordinates x_d, y_d, z_d of each corner given in anticlockwise order as seen from the plasma. The whole R,VR plane must now be explored, but the aperture limitations are not so severe, and the starting point on the cyclotron orbit can be approximately defined by the direction of the line from the point to the plate. Since the plate usually faces the plasma, the direction of the normal to the plane of the plate has been used. If the projected velocity vector of the particle in the plasma meets the plane of the plate, then the point P at which it does is found to lie on the plate in the following way. Let A,B.C.D... be the corners of the plate, and let $\vec{A}_n$, $\vec{B}_n$, $\vec{C}_n$, $\vec{D}_n$ ... be the vectors normal to the sides $\vec{AB}$, $\vec{BC}$, $\vec{CD}$ ... which lie in the plane. Then if all the scalar products $\vec{PA}.\vec{A}_n$, $\vec{PB}.\vec{B}_n$ .. are positive, the point P lies within the area bounded by A, B, C, D ... The function $F(\vec{r}\,\vec{v})$ is defined in this way and the integration to determine E(R,VR) is carried out as before. Contours of E(R,VR) are shown in Fig.14 for a plate 1·9 by 12 cms aligned in the z direction but centred on the y axis 26·5 cms from the plasma centre. The wavy nature of the contours in the diagram is due to the small number of points calculated. This particular case shows some variation of efficiency over the interesting area of the R,VR plane and to act as a true measure of total neutral emission, the detector is placed much closer to the plasma.

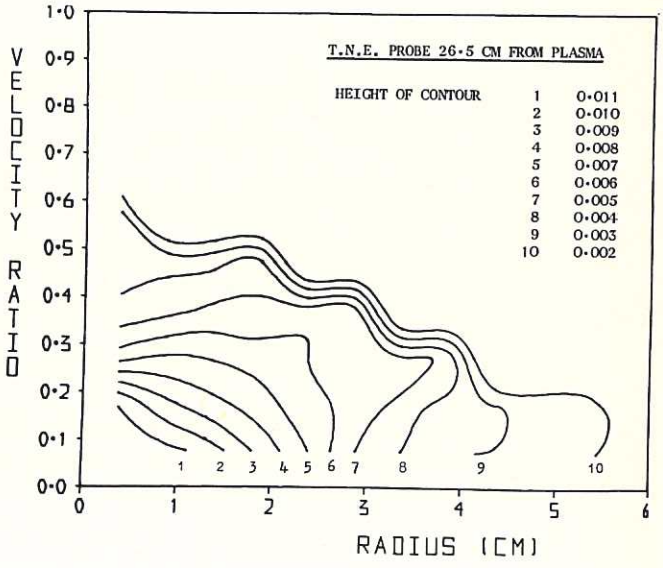

Fig. 14 (CLM-R76)
Detector efficiency map for total neutral emission detector. Plate is 1.9 cm wide in x direction, 12 cms long in z direction and centred on the y axis at 26.5 cms from the plasma.

ACKNOWLEDGEMENTS

All the basic field generating, line integration and interpolation routines used in the programmes described above were written by M. Larkin of the Theory Division. The authors would also like to thank M. Larkin for his help and guidance and to thank Miss M. Rankin for her assistance with the programmes during her visit to the Laboratory from ORNL.

REFERENCES

1. SIAMBIS, J.G. Guiding center motion of particles in combined mirror-multipole cusp magnetic fields. Ann Arbor, Michigan, University Microfilms, 1966. (Reprint of Ph.D Thesis, University of California, 1965).

2. NORTHROP, T.G. and TELLER, E. Stability of the adiabatic motion of charged particles in the earth's field. Phys. Rev., vol.117, no.1, January 1960. pp.215-225.

3. LARKIN, M. Computer programs for the numerical study and graphical display of magnetic fields. London, H.M.S.O., April, 1964. CLM - R 31.

4. TAYLOR, J.B. Equilibrium and stability of plasma in arbitrary mirror fields. Phys. Fluids, vol.7, no.6, June, 1964. pp.767-773.

5. MURPHY, E.G., RIVIERE, A.C. and SWEETMAN, D.R. Radial distribution of plasma formed in simple mirror machines by field ionization of fast neutral atoms. Nucl. Fusion, vol.6, no.3, September, 1966. pp.200-206.

Available from

HER MAJESTY'S STATIONERY OFFICE

49 High Holborn, London, W.C.1
423 Oxford Street, London W.1
13a Castle Street, Edinburgh 2
109 St. Mary Street, Cardiff CF1 1JW
Brazennose Street, Manchester 2
50 Fairfax Street, Bristol 1
258-259 Broad Street, Birmingham 1
7-11 Linenhall Street, Belfast BT2 8AY

or through any bookseller.

Printed in England

S. O. Code No. 91-3-21-46